

# Novel Electrochemical Acetylcholinesterase Biosensor Based on Core-Shell Covalent Organic Framework@Multi-Walled Carbon Nanotubes (COF@MWCNTs) Composite for Detection of Malathion

Xue Wang\*, Shuang Yang, Jiajia Shan, Xuting Bai

School of Ocean Science and Technology, Dalian University of Technology, Panjin, 124221, China

\*E-mail: [wangxue@dlut.edu.cn](mailto:wangxue@dlut.edu.cn)

Received: 10 January 2022 / Accepted: 4 March 2022 / Published: 5 April 2022

In this study, a novel electrochemical acetylcholinesterase (AChE) biosensor based on covalent organic framework@multi-walled carbon nanotubes (COF@MWCNTs) composite was developed for the detection of organophosphorus pesticides (OPs). The COF@MWCNTs was prepared via in-situ formation of COF-DhaTab on the surface of multi-walled carbon nanotubes (MWCNTs) by a facile solvothermal method. The COF@MWCNTs composite displayed a typical core-shell structure, which was used as an ideal host for enzyme immobilization and exhibited strong electron transfer ability in electrochemical sensing. These properties were originated from the synergistic effect of COF and MWCNTs. According to the inhibition effect of malathion toward AChE activity, the sensitive detection of malathion was obtained using the electrochemical AChE biosensor. Under the optimal conditions, the proposed biosensor exhibited a linear range from 1 nM to 10  $\mu$ M with a detection limit of 0.5 nM for malathion determination. The AChE biosensor also showed good anti-interference ability, reproducibility, storage stability. In practice, the biosensor was employed to detect malathion in water and spinach samples with satisfactory recovery.

**Keywords:** Acetylcholinesterase; Electrochemical biosensor; Malathion; Covalent organic frameworks; Core-shell

## 1. INTRODUCTION

In the past decades, various pesticides are being used in agriculture and horticulture to protect crops against pests and diseases for enhancing the yield and quality of crops. The pesticides have become an essential chemical substance for the stable development of the agricultural economy and agricultural products supply. As relatively low toxicity and broad-spectrum insecticide, malathion (diethyl 2-[(dimethoxyphosphinothioyl)thio]butanedioate) is one of the most extensively used organophosphorus

pesticides (OPs). The widespread use of malathion leads to serious pesticide residue problems in vegetables and fruits, causing serious concerns in food safety [1]. In addition, malathion residues in the environmental matrix have been detected in almost all types of environmental samples such as water, soils and sediments [2-4]. The direct exposure to malathion from different routes leads to persistent health risks in mammals and humans. The neurotoxicity, hepatotoxicity, nephrotoxicity, reproductive toxicity and other adverse effects originating from malathion have been reported [5]. Moreover, malathion has genotoxic and carcinogenic potential, which was classified as “probably carcinogenic to humans (Group 2A)” by the International Agency for Research on Cancer (IARC) of the World Health Organization (WHO) [6]. Thus, it is crucial to monitor the concentration level of malathion for standardized usage of pesticides and controlling pesticide residues in agricultural products.

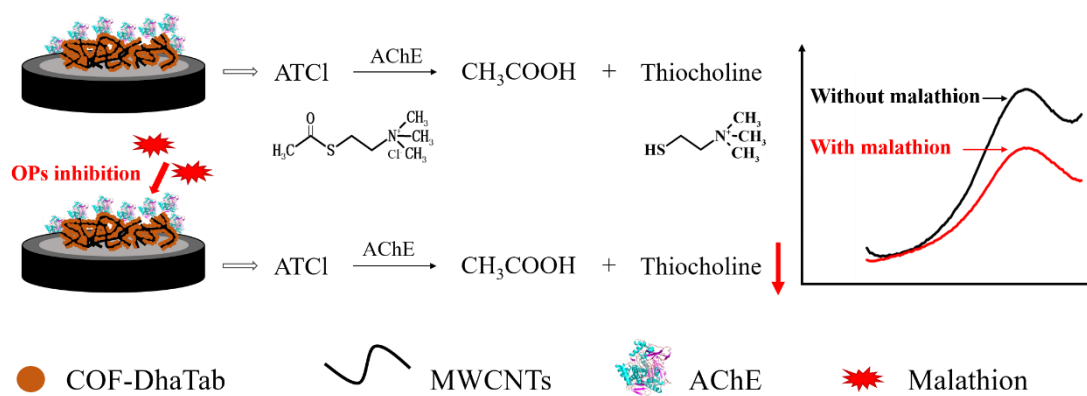
For rapid monitoring of pesticide residues in food and environment, the electrochemical biosensing technique is an emerging candidate. The electrochemical method provides an alternative analytical tool, which is low-cost, rapid, easy to operate and on-site potential [7, 8]. The biosensor can be classified according to the biological recognition elements as enzyme biosensor, nucleic acid biosensor, immunosensor, and so on. Among these biosensors, enzyme biosensors based on enzyme inhibition principle have been greatly developed for the detection of various OPs [9]. For example, the activity of insects' cholinesterase can be inhibited by OPs, consequently the central nervous system is disturbed. This is the reason that OPs are widespread used as insecticides. Thus, acetylcholinesterase (AChE) is the ideal bioreceptor for the fabrication of enzyme biosensors for OPs detection. The detection principle is as follows [10]: Acetylthiocholine chloride (ATCl) can be hydrolyzed into electroactive thiocholine under AChE. When the AChE' activity is strongly inhibited by OPs through non-reversibly bonding, the amount of generated thiocholine decreased. Consequently, the oxidation current of thiocholine is smaller compared to the un-inhibited AChE. The value of inhibition rate can be used to quantify OPs in a certain concentration range.

Based on the above description, the AChE inhibition strategy adopted in electrochemical biosensing is involved in two key processes: (i) the hydrolysis reaction of ATCl with AChE and (ii) the electrochemical oxidation of thiocholine. How to successfully adjust and balance the above two processes is a crucial point for constructing high-performance electrochemical AChE biosensor. The choice of sensing materials must ensure the high activity of AChE and rapid electron transfer at the electrode interface.

In terms of biosensing materials, covalent organic frameworks (COFs) showed promising opportunities in the construction of biosensing platforms, due to its advantages of unique framework structure, large specific surface area, good adsorption capacity and abundant functional groups [11]. The biocatalysis applications of COFs as host platforms for enzyme immobilization are reported [12, 13]. In 2015, Kandambeth et al. firstly reported that a hollow spherical covalent organic framework (COF-DhaTab) was used for trypsin immobilization, showing a high storage capacity of trypsin ( $15.5 \mu\text{mol g}^{-1}$ ) [14]. However, due to their intrinsically low electrical conductivity, COFs have an innate disadvantage in efficient electron transfer, which seriously restricts their electrochemical applications. Thus, the design and usage of functionalized COFs with hybrid nanostructures is attractive for overcoming the major drawback in electrochemical applications [15]. The in-situ formation of COFs on the excellently conducting carbon-based materials such as carbon nanotubes (CNTs) not only maintain the unique

properties of COFs but also enhance the conductivity of hybrid materials. Recently, Sun et al. prepared COF@NH<sub>2</sub>-CNT composite by a one-pot method, and the COF@NH<sub>2</sub>-CNT based electrochemical sensor showed a high sensitivity for the determination of furazolidone in chicken and lamb samples [16]. Wang et al. prepared an electroactive COF<sub>Thi-TPPB</sub> by a dehydration condensation reaction, and the COF<sub>Thi-TPPB</sub> was further capped with NH<sub>2</sub>-CNT to form COF<sub>Thi-TPPB</sub>-CNT composite for fabricating an electrochemical ascorbic acid and pH sensor [17]. To our knowledge, the COF@CNT hybrid material for constructing electrochemical enzyme biosensors was not reported before. We promise that developing a novel pesticide biosensor based on AChE immobilization on the COF@MWCNTs is an interesting attempt.

In this study, the COF@MWCNTs composite was prepared by a solvothermal method in which 2,5-dihydroxyterephthalaldehyde (Dha) and 1,3,5-tris(4-aminophenyl)benzene (Tab) as organic ligands and MWCNTs as supporting material. The as-prepared composite was characterized by scanning electron microscopy (SEM), transmission electron microscopy (TEM), X-ray diffraction (XRD), Fourier-transform infrared spectroscopy (FT-IR) and X-ray photoelectron spectroscopy (XPS). A novel electrochemical acetylcholinesterase (AChE) biosensor based on COF@MWCNTs was fabricated for the determination of malathion, and the detection principle is shown in **Scheme 1**. The cyclic voltammetry (CV), differential pulse voltammetry (DPV) and amperometric measurements were performed to optimize the experimental conditions and investigate the analytical performances of the biosensors. The linear relationship between inhibition rate and concentration of malathion was established for quantitative analysis. The anti-interference ability, reproducibility, stability and application in real samples were also demonstrated.



**Scheme 1.** Schematic representation of the detection principle of malathion using the proposed electrochemical AChE biosensor.

## 2. EXPERIMENTAL

### 2.1 Chemicals

Acetylcholinesterase (AChE) from *Electrophorus electricus* (electric eel), acetylthiocholine chloride (ATCl, purity  $\geq 99\%$ ) and malathion were purchased from Sigma-Aldrich (Shanghai, China).

2,5-dihydroxyterephthalaldehyde (Dha), 1,3,5-tris(4-aminophenyl)benzene (Tab), 1,2-dichlorobenzene (*o*-DCB), 1-butanol and tetrahydrofuran (THF) were purchased from J&K Scientific Ltd. (Beijing, China). Multi-walled carbon nanotubes (MWCNTs, OD: 30-50 nm, length: 10-20  $\mu\text{m}$ , purity: >98 wt%) were purchased from Chengdu Organic Chemicals Co. Ltd., Chinese Academy of Sciences. All other chemicals used in this work were of analytical grade.

## 2.2. Instruments

The morphological characterizations of the prepared materials were performed using scanning electron microscopy (SEM) on Nova NanoSEM 450 microscope (FEI, USA) and transmission electron microscopy (TEM) on Tecnai G<sup>2</sup> F30 microscope (FEI, USA). The X-ray diffraction (XRD) data were collected using an XRD-7000S X-ray diffractometer (Shimadzu, Japan). The scanning range is 2–40° with a scanning rate of 5°/min. X-ray photoelectron spectroscopy (XPS) was obtained using ESCALAB 250Xi (Thermo Fisher Scientific, USA). Fourier-transform infrared spectroscopy (FT-IR) was recorded on a Nicolet iN10 MX & iS10 spectrometer over the wavenumber range of 650–4000  $\text{cm}^{-1}$  (Thermo Fisher Scientific, USA)

## 2.3 Preparation of COF-DhaTab

The COF-DhaTab was prepared by using a solvothermal method according to previous research with minor modification [18]. The 0.24 mmol Dha and 0.16 mmol Tab were dispersed in acetic acid (6 M, 0.6 mL)/1-butanol (1.5 mL)/*o*-DCB (1.5 mL) mixed solution, respectively. Then the above solution was sonicated in order to obtain a homogenous dispersion and adequately mixed into a Teflon-lined autoclave. The autoclave was sealed and heated at 120°C for 72 h. A reddish orange-colored precipitate was formed and washed in THF and ethanol under magnetic stirring for 24 h. Finally, the prepared COF-DhaTab powder was dried under vacuum overnight.

## 2.4 Preparation of COF@MWCNTs composite and COF@MWCNTs modified electrode

The preparation method was similar to the procedure of COF-DhaTab preparation. Firstly, 12 mg of MWCNTs was dispersed in 1-butanol/*o*-DCB mixed solution. Then, the above solution was mixed into acetic acid solution containing 0.24 mmol Dha and 0.16 mmol Tab to get a homogenous dispersion. After that, the whole reaction solution was poured into an autoclave and heated at 120°C for 72 h. The prepared precipitate was washed and dried under vacuum. The obtained product was denoted as COF@MWCNTs.

In order to prepare COF@MWCNTs modified electrode, 10  $\mu\text{L}$  of the suspension containing 0.5  $\text{mg mL}^{-1}$  COF@MWCNTs and 0.1% chitosan was dropped on the clean surface of glassy carbon electrode. The modified electrode was dried at room temperature for the next enzyme immobilization. Then, 10  $\mu\text{L}$  of the AChE solution (50  $\text{U mL}^{-1}$  AChE and 0.1% chitosan) was coated on the

COF@MWCNTs modified electrode. The enzyme electrode was dried in the refrigerator at 4°C and kept for further measurements. The fabricated electrode was named as AChE/COF@MWCNTs/GCE.

### 2.5 Electrochemical measurements

The electrochemical measurements were operated on a CHI 660E electrochemical workstation (Shanghai Chenhua, China). A typical three-electrode system was used, wherein a GCE as the working electrode, an Ag/AgCl electrode as the reference electrode, and a Pt wire electrode as the auxiliary electrode. The cyclic voltammetry (CV) measurement for electrochemical characterization was carried out in 1 mM  $[\text{Fe}(\text{CN})_6]^{3-}/[\text{Fe}(\text{CN})_6]^{4-}$  solution containing 0.1 M KCl in the range of -0.2 to +0.6 V at a scan rate of 50 mV/s. The amperometric measurement was carried out in 0.1 M PBS (pH = 7.0) at a constant potential of +0.7 V by adding different concentrations of ATCl solution. The differential pulse voltammetry (DPV) method was carried out in 1 mM ATCl solution in the range of +0.3 to +0.85 V.

DPV was used for the determination of malathion. The DPV curve was recorded on the AChE/COF@MWCNTs/GCE in 0.1 M PBS containing 1 mM ATCl. In the malathion inhibition study, the fabricated AChE biosensor was firstly dipped in different concentrations of malathion solution for 10 min. Then, the DPV measurement was carried out on the inhibited AChE biosensor in 1 mM ATCl solution. The inhibition rate was calculated as the following equation (1), where  $I_0$  and  $I_i$  are the oxidation peak current of ATCl before and after malathion inhibition, respectively. The inhibition rate and the concentration of malathion had a linear relationship within a certain concentration range.

$$\text{Inhibition (\%)} = (I_0 - I_i)/I_0 \times 100\% \quad (1)$$

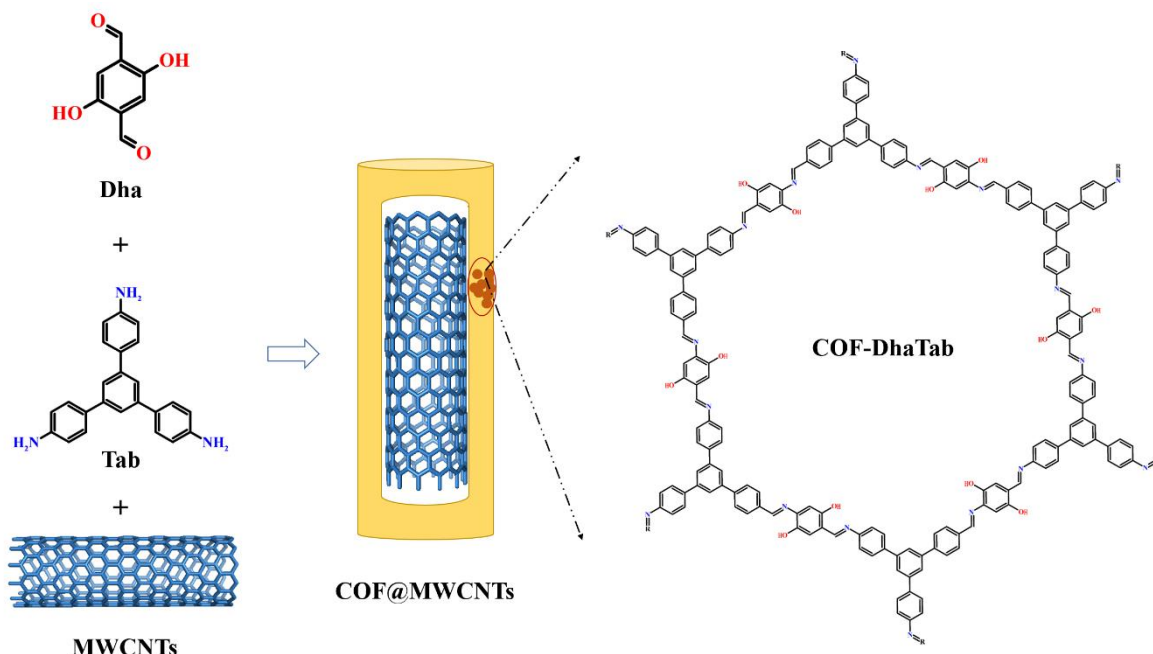
### 2.6 Pretreatment of real samples

To evaluate the practicability of the electrochemical biosensor, tap water and spinach were chosen as real samples. Before detection, the pretreatment of real samples was performed. The tap water sample was filtered with an aqueous phase filter membrane to remove the potentially suspended solids. For the spinach sample, firstly, 20 g of spinach was grinded to get a homogeneous suspension. Anhydrous sodium sulfate and activated carbon were added into the suspension for dehydration and decolorization. Then, the sample was placed in a conical flask and extracted with 100 mL acetonitrile and 5 g NaCl under stirring at a rotating speed of 150 r/min for 12 h. The sample was extracted three times. The supernatant was collected after centrifugation, and filtered with 0.22  $\mu\text{m}$  filter membrane. The extract was evaporated and the residue was dissolved in 2 mL methanol for further determination.

## 3. RESULTS AND DISCUSSION

### 3.1 Preparation and characterization of COF-DhaTab and COF@MWCNTs

Dha and Tab as the building blocks were used to synthesize COF-DhaTab via Schiff base condensation reaction by a solvent thermal method. The core-shell structured COF@MWCNTs was prepared by the in-situ growth of COF-DhaTab on the MWCNTs surface (**Scheme 2**).



**Scheme 2.** Synthesis route of COF@MWCNTs.

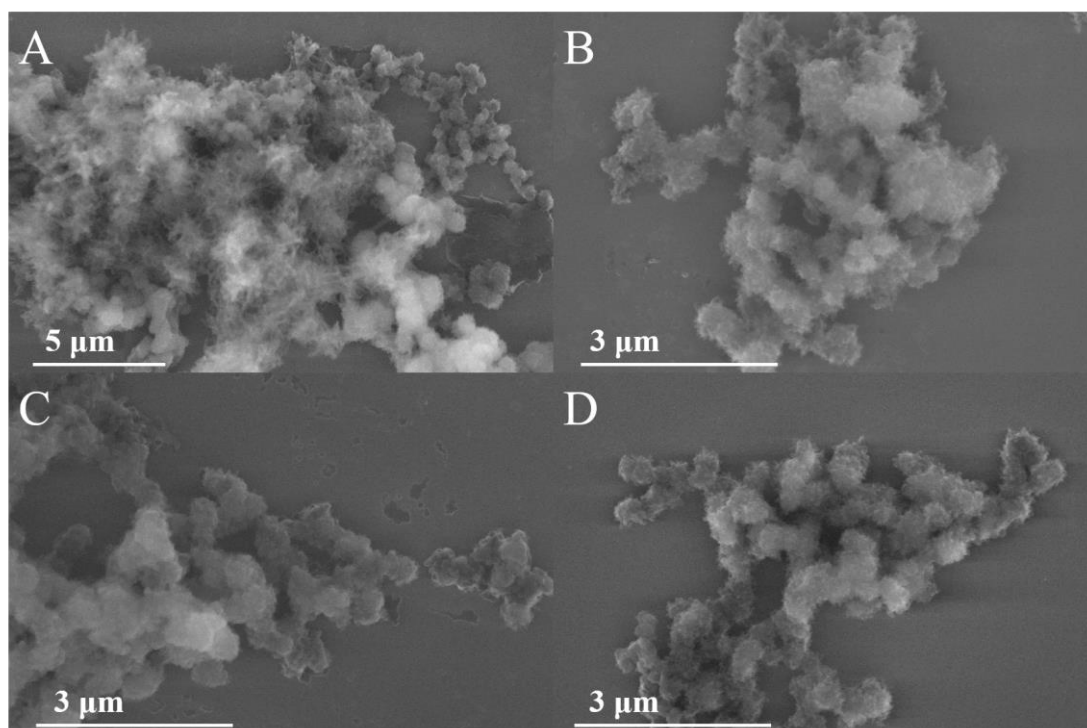


**Figure 1.** SEM images of (A) COF-DhaTab 12 h, (B) COF-DhaTab 24 h, (C) COF-DhaTab 36 h, (D) COF-DhaTab 48 h.

The morphological characterizations of COF-DhaTab and COF@MWCNTs were studied by SEM and TEM (**Figure 1** and **Figure 2**). At a short reaction time (12 h), the aggregated microparticles were displayed on the COF-DhaTab-12h. As the reaction time increased from 12 to 72 h, the microcrystals continued to aggregate and the structure of COF-DhaTab sample became more uniform

and regular. The COF-DhaTab-72h showed spheroid structures with rough surfaces connecting to each other with a diameter from 300 to 600 nm [14].

After the COF-DhaTab was grafted on the surface of MWCNTs, COF@MWCNTs showed a rod-like structure similar to MWCNTs (**Figure 2B**). For further confirming preparation of the hybrid, the detailed morphology of MWCNTs and COF@MWCNTs was observed using TEM (**Figure 2E** and **2F**). A larger diameter (120 – 170 nm) of COF@MWCNTs was observed compared to MWCNTs (30 – 50 nm). In addition, spherical nanoparticles of COF-DhaTab were uniformly distributed on the MWCNTs. **Figure 2C** and **2D** showed the SEM images with the different magnification of AChE molecules loaded on COF@MWCNTs. The core-shell structure of COF@MWCNTs provided large surface area and enzyme immobilization sites, which is favorable for the efficient incorporation of AChE and COF@MWCNTs to fabricate a highly sensitive electrochemical biosensor.

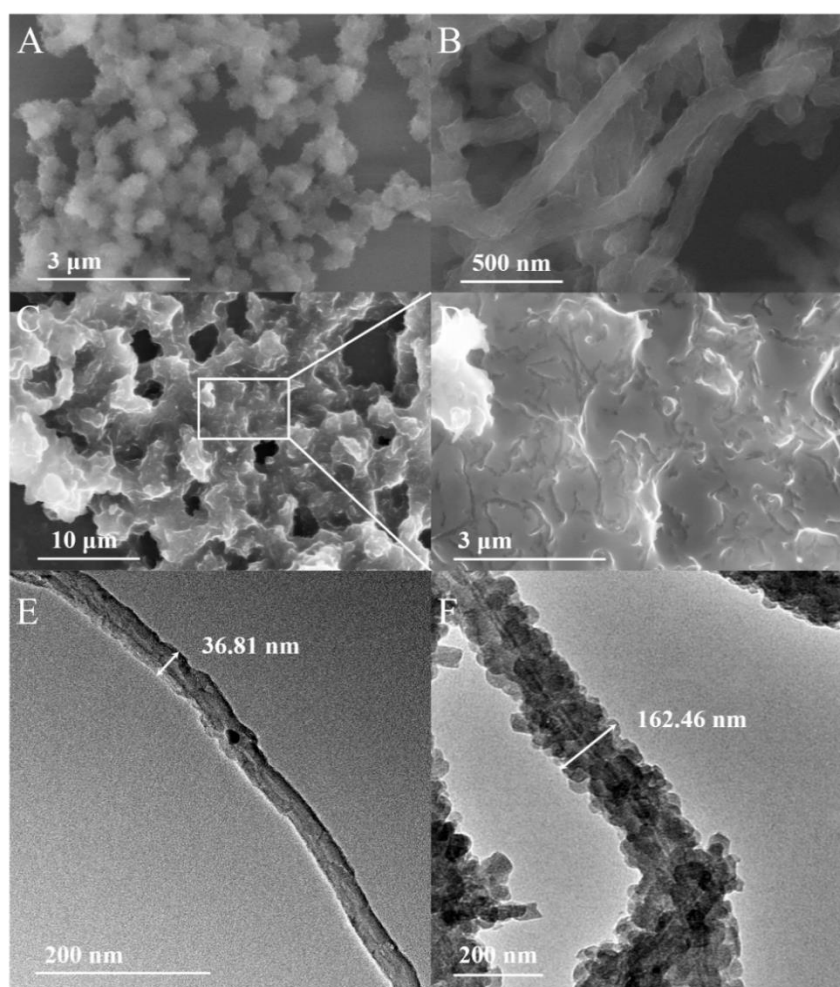


**Figure 2.** SEM images of (A) COF-DhaTab-72h, (B) COF@MWCNTs, (C) AChE/COF@MWCNTs and (D) enlarged view of AChE/COF@MWCNTs; TEM images (E) MWCNTs and (F) COF@MWCNTs.

The time dependence of preparation of COF-DhaTab was further studied by XRD analysis (**Figure 3A**). The XRD patterns of COF-DhaTab for 12 ~ 72 h of reaction time had similar characteristic peaks, which indicated that a shorter time is enough for the COF-DhaTab crystallite formation. As the

reaction progresses, the crystallites are gradually self-assembled into a spherical structure. The intense and sharp diffraction (100) at  $2\theta = 2.80^\circ$  demonstrated the high crystallinity of COF-DhaTab. Other peaks at  $4.84^\circ$ ,  $5.58^\circ$ ,  $7.40^\circ$  and  $9.82^\circ$  were indexed to the (110), (200), (120) and (220) reflections respectively [19]. The XRD results of individual MWCNTs and COF@MWCNTs were shown in **Figure 3B**. The diffraction peak at  $2\theta = \sim 26^\circ$  in the XRD pattern of MWCNTs was the (002) plane of the hexagonal graphite structure [20]. The XRD pattern of COF@MWCNTs was almost the same as COF, indicating that the addition of MWCNTs (12 and 24 mg) in the synthesis of COF@MWCNTs had no effect on the formation of COF-DhaTab crystallite. The surface of MWCNTs had been completely covered by the COF-DhaTab. The result showed again that the MWCNTs played a role of carrier and the COF-DhaTab was successfully synthesized on MWCNTs.

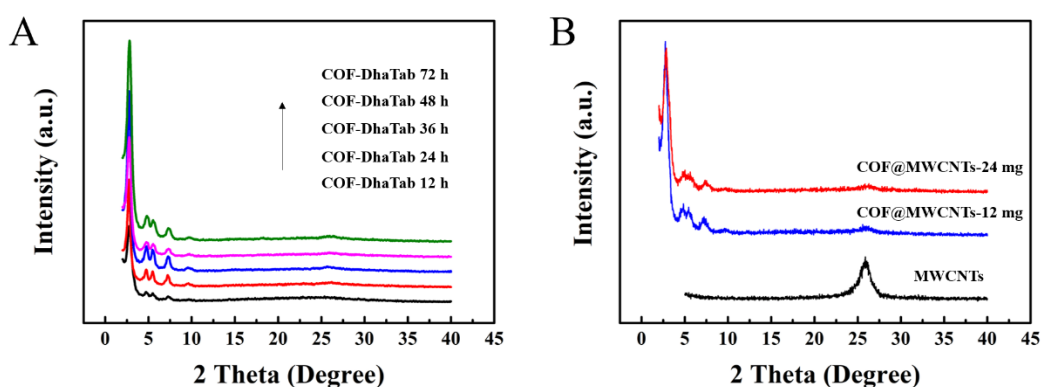


**Figure 3.** The XRD patterns of (A) COF-DhaTab at different reaction time and (B) MWCNTs, COF@MWCNTs (24mg MWCNTs) and COF@MWCNTs (12mg MWCNTs)

The FT-IR spectra of COF-DhaTab and its monomers (Dha and Tab) were shown in **Figure 4A**. The N-H stretching band at  $3433.1$  and  $3353.6$   $\text{cm}^{-1}$  for Tab monomer and the C=O stretching vibration band at  $1665.2$   $\text{cm}^{-1}$  for Dha monomer were observed in the FT-IR spectra [21]. Meanwhile, the newly formed peak at  $1613.1$   $\text{cm}^{-1}$  belonging to C=N band [22] in the COF-DhaTab was accompanied by the disappearance of the characteristic peaks of the N-H stretching band and the C=O stretching vibration band. This result indicated that the COF-DhaTab was successfully synthesized through the Schiff base condensation reaction between Dha and Tab monomers. The characteristic peaks of FT-IR spectra of COF-DhaTab for the different reaction times of 12, 24, 36 and 48 h (**Figure 4B**) were consistent with COF-DhaTab 72h, which corresponded to the XRD results at different times. The FT-IR spectra of COF@MWCNTs (**Figure 4C**), especially when the additive amount of MWCNTs was 12 mg, proved the above conclusion that the formation of COF-DhaTab in the composite.

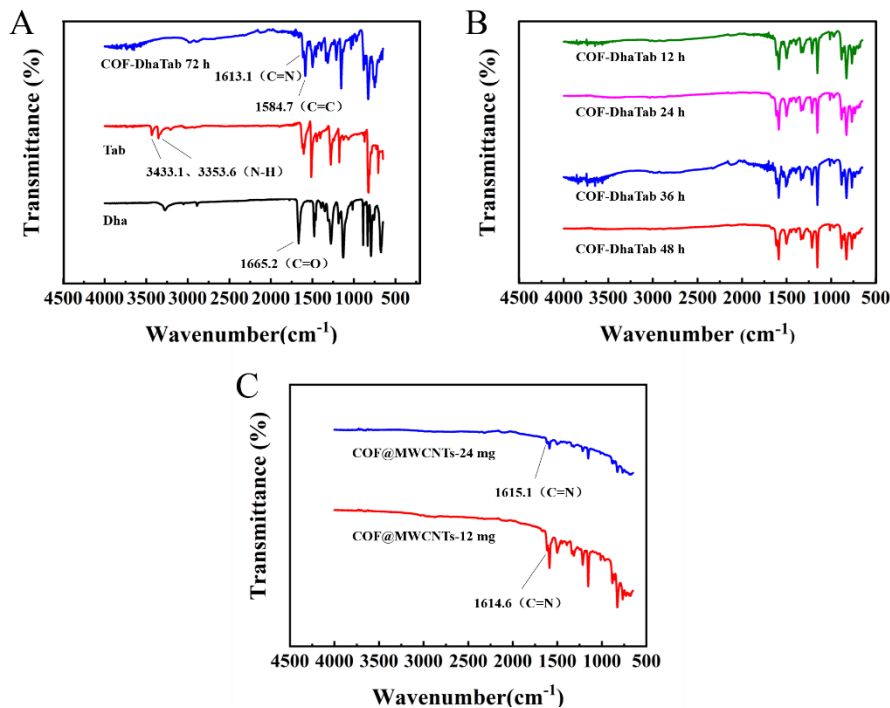


**Figure 4.** The FT-IR spectra of (A) Tab, Dha and COF-DhaTab 72h, (B) COF-DhaTab for different reaction time of 12, 24, 36 and 48 h and (C) COF@MWCNTs (24 mg MWCNTs) and COF@MWCNTs (12 mg MWCNTs).

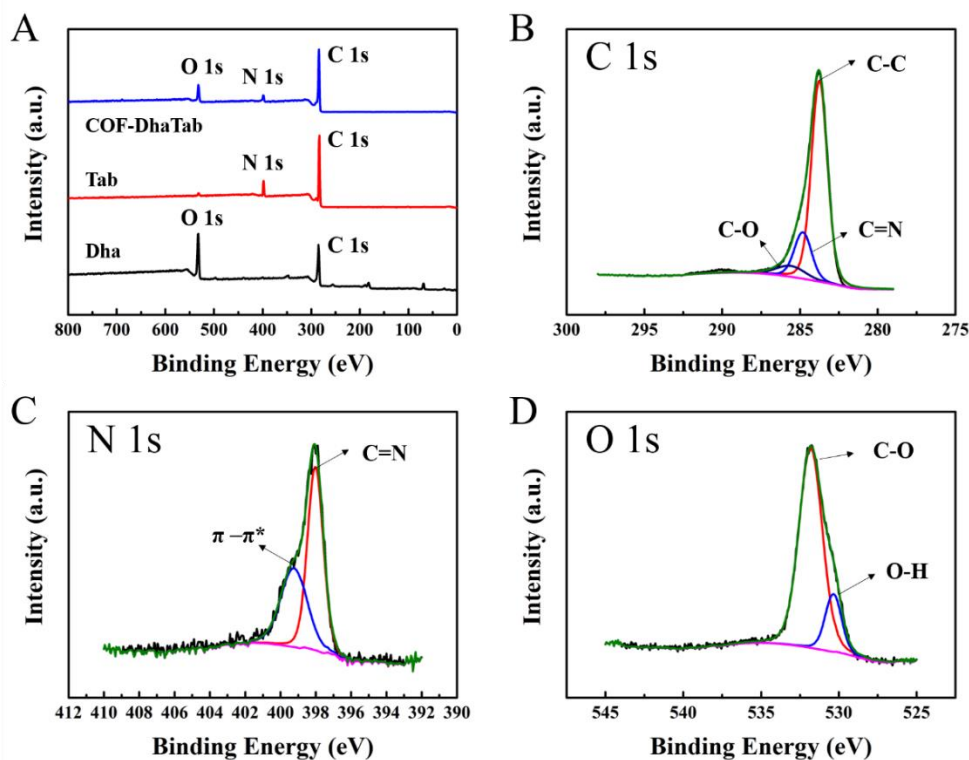


**Figure 5.** (A) XPS spectra of COF-DhaTab, Tab and Dha; (B-D) High-resolution XPS spectra for C 1s, N 1s and O 1s of COF-DhaTab.

XPS was used to confirm the chemical composition of COF-DhaTab. The comparison of XPS spectra for the prepared COF-DhaTab and the monomers (Tab and Dha) was shown in **Figure 5A**. The full XPS spectra of COF-DhaTab indicated the existence of O, N, C elements of COF-DhaTab from the O, N of Tab and O, C of Dha. Further study was carried out from the high-resolution XPS spectra for C 1s, N 1s and O 1s of COF-DhaTab. The C 1s spectrum of COF-DhaTab was fitted to three peaks. The fitting peaks were located at 285.31 eV, 284.72 eV, 283.75 eV, which were assigned to C-O, C=N, C-C [23]. Two peaks at 399.27 eV and 398.03 eV were shown in the N 1s spectrum, which were assigned to  $\pi$ - $\pi^*$  and C=N. Two peaks at 531.81 eV and 530.35 eV were shown in the O 1s spectrum, which were assigned to C-O and O-H from Dha monomer. The XPS results adequately confirmed the formation of COF-DhaTab.

### 3.2 Electrochemical behavior of the AChE/COF@MWCNTs/GCE biosensor

The electrochemical characterization of the electrodes was performed by CV using  $[\text{Fe}(\text{CN})_6]^{3-}/[\text{Fe}(\text{CN})_6]^{4-}$  as a redox probe. As shown in **Figure 6A**, a pair of redox peaks were seen at the bare GCE (curve a). The obvious decrease of current at COF-DhaTab/GCE (curve b) was ascribed to the poor conductivity of COFs. The largest current was obtained at COF@MWCNTs/GCE (curve c). That reason was the unique core-shell structure of COF@MWCNTs composite providing high specific surface area and good electrical conductivity from carbon-based material [24], which was beneficial for facilitating the electron transfer. The enzyme-modified electrode (AChE/COF@MWCNTs/GCE, curve d) showed a lower current due to the low conductivity of AChE molecules, which also proved the successful fabrication of AChE/COF@MWCNTs/GCE.

The DPV was utilized to investigate the electrochemical responses at different AChE modified electrodes for ATCl (**Figure 6B**). Oxidation current peaks were seen at AChE/GCE (curve a), AChE/COF-DhaTab/GCE (curve b), AChE/COF@MWCNTs/GCE (curve c), respectively. The current peaks were ascribed to the oxidation of thiocholine, which was generated from hydrolysis of ATCl under enzymatic reaction by AChE [9]. The current values were as follows:  $I(\text{AChE/COF@MWCNTs/GCE}) > I(\text{AChE/COF-DhaTab/GCE}) > I(\text{AChE/GCE})$ . The reason was the effective immobilization of AChE on COF@MWCNTs/GCE and the enhanced electrochemical response of thiocholine by COF@MWCNTs composite.

The CV curves of AChE/COF@MWCNTs/GCE in 1 mM ATCl solution at scan rates (10 to 200 mV/s) were recorded in **Figure 6C**. **Figure 6D** showed a good linear relationship between the oxidation current (y) and scan rate (x), and the regression equation is  $y = 0.03394x + 2.60185$  ( $R^2=0.99027$ ), indicating the electrochemical reaction at AChE/COF@MWCNTs/GCE was an adsorption-controlled process [25].

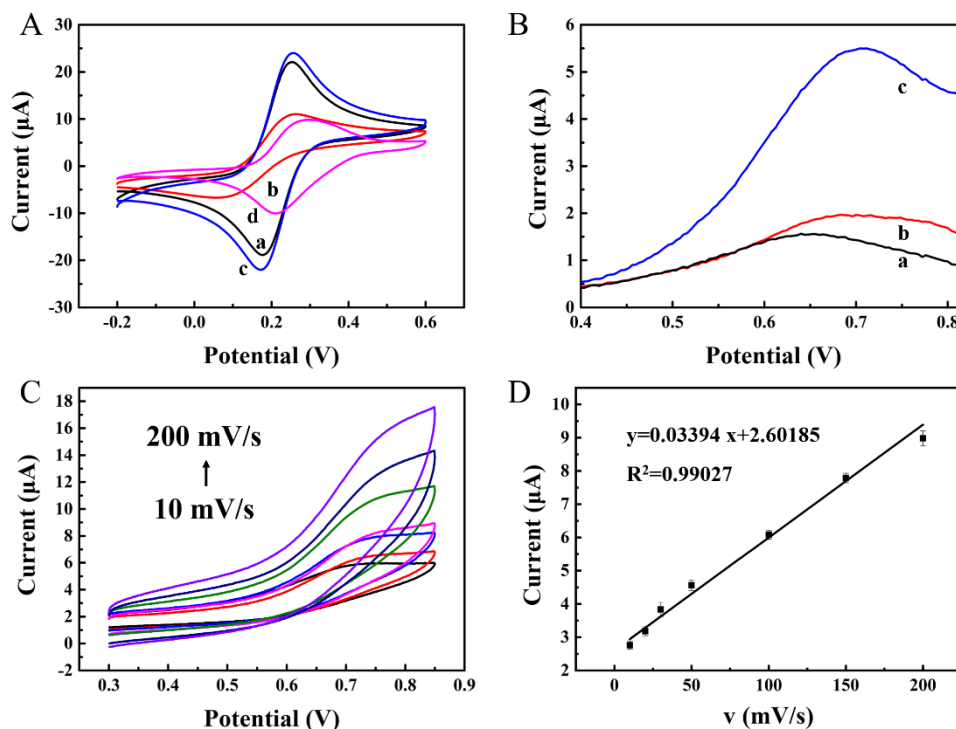


**Figure 6.** (A) CV responses of (a) bare GCE, (b) COF-DhaTab/GCE, (c) COF@MWCNTs/GCE, (d) AChE/COF@MWCNTs/GCE in 1 mM  $[\text{Fe}(\text{CN})_6]^{3-}/[\text{Fe}(\text{CN})_6]^{4-}$  solution containing 0.1 M KCl; (B) DPV responses of (a) AChE/GCE, (b) AChE/COF-DhaTab/GCE, (c) AChE/COF@MWCNTs/GCE in 0.1 M PBS (pH 7.0) containing 1 mM ATCl; (C) CV responses of AChE/COF@MWCNTs/GCE for 1 mM ATCl at scan rates from 10 to 200 mV/s; (D) the calibration curve between oxidation current of ATCl and scan rates.

### 3.3 Optimization of the experimental parameters

In the preparation process of the COF@MWCNTs composite, the amount of MWCNTs had significant effects on the electrical conductivity. In this core-shell structure, the MWCNTs as a carrier also affect the formation of COF in terms of amount and morphology. Thus, the amount of MWCNTs in the range of 0 to 24 mg was optimized in this study. As shown in **Figure 7A**, the oxidation current increased with the addition of MWCNTs, and reached a plateau over 12 mg of MWCNTs. This demonstrated that the cooperation of MWCNTs encouraged the oxidation of thiocholine at the COF-modified electrode. Thus, 12 mg of MWCNTs was adopted in this study.

The oxidation currents of the as-prepared biosensor at different pH (6.0 to 8.5) were measured (**Figure 7B**). The enzymatic activity of AChE, enzyme-catalyzed reaction of ATCl and oxidation reaction of thiocholine were all influenced by pH value. The maximum current was obtained at pH 7.0 [26]. Thus, pH 7.0 was selected as the optimal pH for the further electrochemical measurements.

The modified amount of COF@MWCNTs and the loading amount of AChE were also optimized. In **Figure 7C**, the current increased with the concentration of COF@MWCNTs before 0.5 mg/mL, and the current no longer obviously increased when the concentration continued to increase. The oxidation current was enhanced by COF@MWCNTs hybrid, but the excess modified materials would cause

stacking of nanomaterials, which hindered the electron transfer. Similarly, the generated thiocholine was influenced by the AChE loading amount, while excess nonconductive enzyme molecules would also hinder the electron transfer. As shown in **Figure 7D**, the maximum current was obtained when the loading amount of AChE was 0.5 U for one individual biosensor. The optimal modified amounts were 0.5 mg/mL for COF@MWCNTs and 0.5 U for AChE.

The concentration of ATCl as reaction substrates was also optimized to get high performance biosensor (**Figure 7E**). The oxidation current reached a high response at 1 mM ATCl, and the further increasing concentration didn't make the current increase significantly, which could be due to the substrates being saturated for the AChE enzyme. Thus, 1 mM ATCl was selected as the substrate in the further experiment.

The inhibition time was an important factor for the inhibition rate of the AChE biosensor. The as-prepared biosensor was incubated in 1  $\mu$ M malathion solution for 2 to 14 min. The inhibition rate of different inhibition time was calculated by equation (1), and the results were shown in **Figure 7F**. The inhibition rate increased significantly with the long inhibition time from 2 to 10 min. The irreversible binding between malathion and AChE was saturated, causing the change of inhibition rate became gentle over 10 min. Hence, 10 min was used as the incubation time.

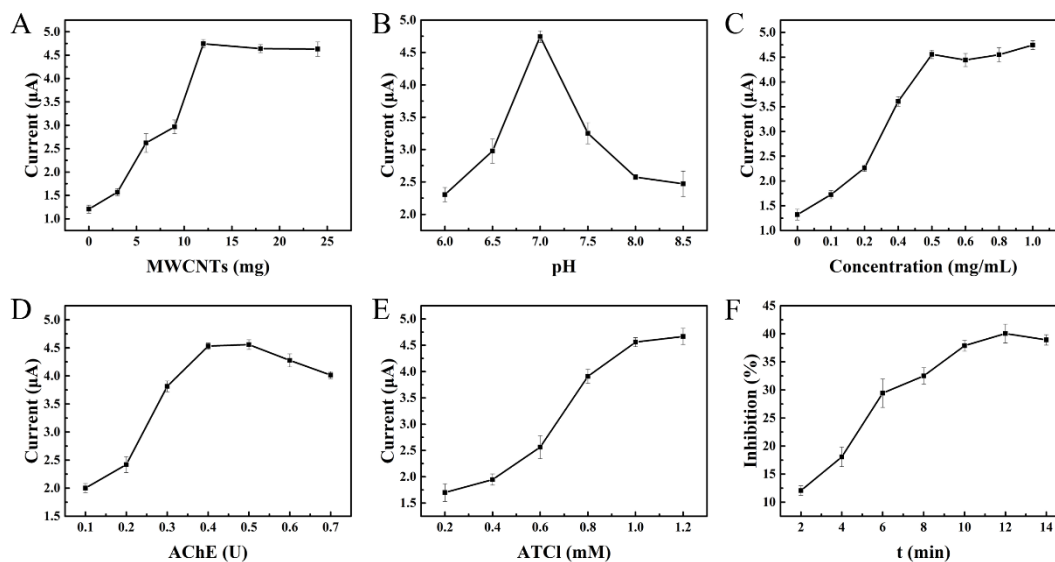


**Figure 7.** Influence of (A) MWCNTs content, (B) pH value, (C) COF@MWCNTs concentration, (D) AChE amount, (E) ATCl concentration, (F) inhibition time.

### 3.4 Amperometric response of the AChE/COF@MWCNTs/GCE biosensor

The amperometric measurement was performed on the AChE/COF@MWCNTs/GCE biosensor at a constant potential of +0.7 V by successive addition of ATCl in the electrochemical cell. The current-time curve of ATCl was shown in **Figure 8**. A linear relationship between oxidation current and ATCl concentration was obtained in the range of 10 to 410  $\mu$ M, and the equation was  $I (\mu\text{A}) = 0.00304c (\mu\text{M}) + 0.23666$  ( $R^2=0.99689$ ). In order to evaluate the affinity between enzyme (AChE) and substrate (ATCl),

apparent Michaelis-Menten constant ( $K_m$ ) was calculated by the Lineweaver-Burk equation (2), where  $I_{ss}$  is the steady-state current after the addition of ATCl,  $I_{max}$  is the maximum current under saturated concentration, and  $C$  is the concentration of ATCl [27].

$$\frac{1}{I_{ss}} = \frac{K_m}{I_{max}} \times \frac{1}{C} + \frac{1}{I_{max}} \quad (2)$$

The reciprocal of oxidation current was as the y value and the reciprocal of concentration was as the x value. The double reciprocal curve was obtained in inset (b), and the equation was  $y$  ( $\mu A^{-1}$ ) =  $177.26919x$  ( $\mu M^{-1}$ ) +  $0.28492$  ( $R^2=0.97558$ ). According to the slope of the double reciprocal curve, the  $K_m$  of this as-prepared biosensor was calculated as  $0.622$  mM, which is similar to  $0.7$  mM obtained from AChE-Er-GRO-Nafion/GCE [28] and  $0.73$  mM obtained from AChE-pRGO-CHIT/GCE [29].

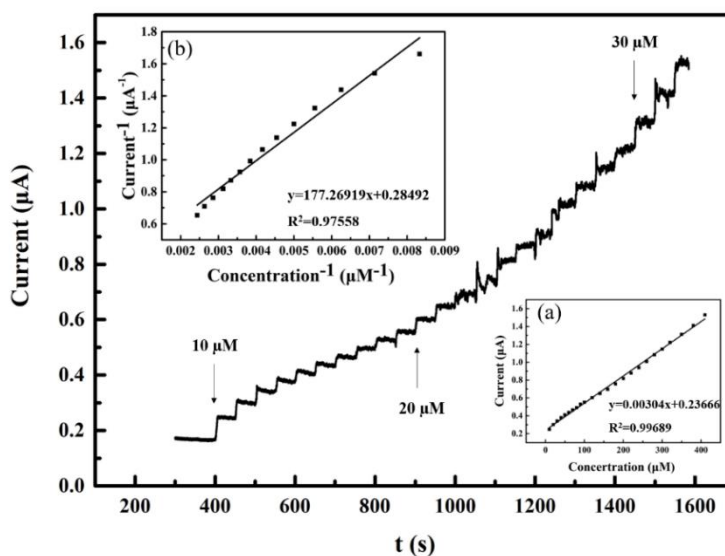


**Figure 8.** Amperometric response of AChE/COF@MWCNTs/GCE by successive additions of ATCl; Inset: (a) the calibration curve between response current and ATCl concentration, (b) Lineweaver-Burk plot of the current<sup>-1</sup> ( $\mu A^{-1}$ ) and ATCl concentration<sup>-1</sup> ( $\mu M^{-1}$ ).

### 3.5 Determination of malathion by the AChE/COF@MWCNTs/GCE biosensor

The DPV method was used to determine malathion based on enzyme inhibition. The activity of AChE was inhibited by organophosphorus pesticide malathion, leading to less thiocholine generated from ATCl. Thiocholine was an electroactive chemical, showing a high oxidation current. The decrement of thiocholine oxidation current reflected the decline of the enzyme activity. In other words, the inhibition rate had a relationship with the inhibition effect from malathion. Hence, the quantitative relation between inhibition rate and malathion concentration was discussed in this study. Under optimal experimental conditions, the DPV curves of the AChE/COF@MWCNTs/GCE biosensor in  $1$  mM ATCl solution after incubation in different concentration of malathion solution ( $0$ ,  $1 \times 10^{-9}$ ,  $1 \times 10^{-8}$ ,  $1 \times 10^{-7}$ ,  $5 \times 10^{-7}$ ,  $1 \times 10^{-6}$ ,  $5 \times 10^{-6}$ ,  $1 \times 10^{-5}$  mol/L) for  $10$  min were shown in **Figure 9A**. The inhibition rate and the logarithm of malathion concentration had a linear relationship in the range of  $1 \times 10^{-9}$  to  $1 \times 10^{-5}$  mol/L, and the calibration curve was shown in **Figure 9B**. The linear fitting equation was Inhibition (%) =

$7.76461 \log c \text{ (mol/L)} + 83.57282$  ( $R^2=0.99513$ ). The LOD was calculated to be  $5 \times 10^{-10}$  mol/L. The AChE biosensor in this work was compared to other sensors (colorimetric, fluorescent and electrochemical sensors), and the linear range and LOD for malathion detection were listed in **Table 1**. The proposed AChE biosensor showed good analytical performances in the detection range and LOD, which proved this enzyme inhibition strategy exhibited high performance for the detection of malathion. The core-shell COF@MWCNTs composite provided a biocompatible microstructure for enzyme immobilization and good conductivity for electrochemical oxidation of thiocholine.

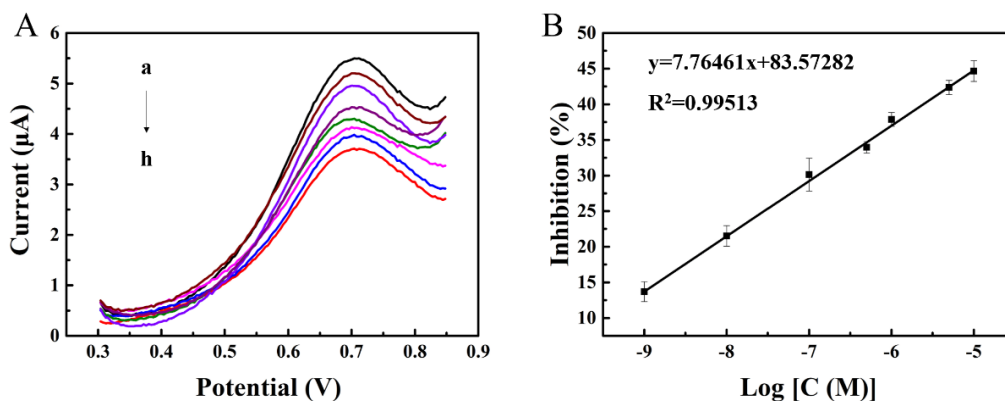


**Figure 9.** (A) DPV curves of the AChE/COF@MWCNTs/GCE biosensor in 1 mM ATCl solution after incubation in different concentrations of malathion solution (a-h: 0,  $1 \times 10^{-9}$ ,  $1 \times 10^{-8}$ ,  $1 \times 10^{-7}$ ,  $5 \times 10^{-7}$ ,  $1 \times 10^{-6}$ ,  $5 \times 10^{-6}$ ,  $1 \times 10^{-5}$  mol/L) for 10 min; (B) The relationship between inhibition rate and malathion concentration.

**Table 1.** Comparison with other sensing platforms for the detection for malathion

Method	Sensing material	Linear range (nM)	LOD (nM)	Ref.
Colorimetric	$\text{Cu}^{2+}$ -g- $\text{C}_3\text{N}_4$	2.2-25	1.204	[30]
	$\text{Ag}_3\text{PO}_4/\text{UiO}-66$	25.1-16100	22.7	[31]
	NiAg/His-GQD/GO	30.27-363	9.38	[32]
Fluorescent	$\text{Cu}^{2+}$ -g- $\text{C}_3\text{N}_4$	70-800	6.798	[30]
	UCNPs-GNPs-PDDA	10-1000	1.42	[33]
	$\beta$ -CD@AgNPs	302.7-75680	30.27	[34]
Electrochemical	Ag-rGO- $\text{NH}_2$	19.1-233	13.6	[35]
	rGO-TEPA-Cu NWs	3.03-60500	1.18	[36]
	CHIT-g-PANI	2000-62500	3800	[37]
	AuNP-CS-IL	0.89-44.6	0.68	[38]
	AChE/CS/ $\text{Fe}_3\text{O}_4$	0.5-20	0.3	[39]
	AChE/COF@MWCNTs	1-10000	0.5	This work

### 3.6 Interference study, reproducibility and stability

Heavy metals are one of the most widespread environmental contaminants, arising from various sources such as agriculture, mining and industry. The pollution of heavy metals in environment caused continuing public health concerns [40]. The environmental samples (water, soil, sediment) [41, 42] and agricultural plants (fruit, vegetable, cereal) [43, 44] are often co-contaminated by heavy metals and pesticides. Meanwhile, some heavy metal ions can form thiol linkages with the serine of AChE and competitively bind at the active sites of AChE, consequently showing a similar enzyme inhibition effect. In order to investigate the interference of heavy metals, AChE biosensors were incubated in 1  $\mu\text{M}$  malathion solution containing 1 mM heavy metals ( $\text{Cu}^{2+}$ ,  $\text{Fe}^{3+}$ ,  $\text{Cd}^{2+}$ ,  $\text{Pb}^{2+}$ ,  $\text{Hg}^{2+}$ ,  $\text{Cr}^{3+}$ ). The inhibition rates of individual malathion and malathion-heavy metal mixed solutions were compared in **Figure 10**. The inhibition rate of individual malathion was regarded as 100%.  $\text{Hg}^{2+}$  showed a relatively strong co-inhibition with malathion, which inhibition rate was 13.9% more than individual malathion. The change of inhibition rate of malathion containing  $\text{Cu}^{2+}$ ,  $\text{Fe}^{3+}$ ,  $\text{Cd}^{2+}$ ,  $\text{Pb}^{2+}$ ,  $\text{Cr}^{3+}$  was below  $\pm 10\%$ , indicating that the biosensor for malathion detection had good anti-interference ability against most heavy metal ions.

The reproducibility of the biosensor was evaluated by recording the DPV response of ten parallel electrodes under the optimal conditions. The RSD was calculated to be 2.19%, indicating good reproducibility. The storage stability is also important for the practical application of the biosensor. In order to evaluate the stability of the biosensor, the as-prepared biosensor was kept in a refrigerator at 4°C. The electrochemical response remained 82.9% of the initial current before storage.

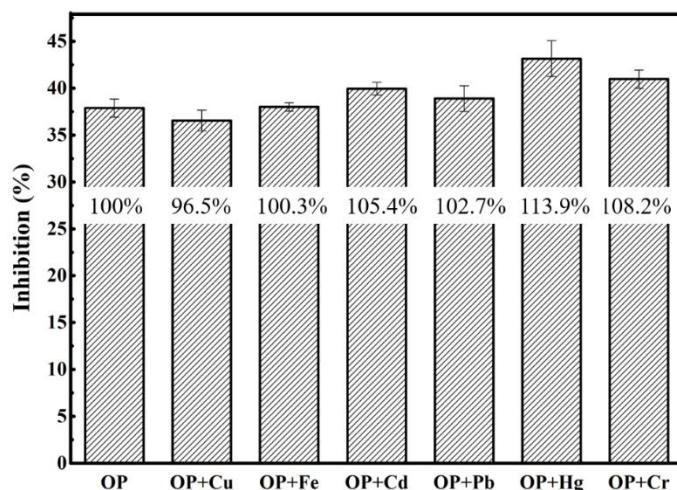


**Figure 10.** The inhibition rates of individual malathion and malathion-heavy metal mixed solution.

### 3.7 Detection of malathion in real samples

In order to prove the applicability of the biosensor for real samples, the recovery rates were measured by standard addition method in tap water and spinach samples (**Table 2**). The recovery rate of

AChE/COF@MWCNTs/GCE biosensor for tap sample was 96.0% to 101.6%, and the RSD was less than 4.5%. The recovery rate of AChE/COF@MWCNTs/GCE biosensor for spinach sample was 98.0% to 105.0%, and the RSD was less than 3.0%. The results of recovery studies indicated that the biosensor had accuracy and reliability in real sample analysis.

**Table 2.** Recovery studies of malathion in real samples.

Samples	Detected (M)	Added (M)	Found (M)	Recovery (%)	RSD (%)
Tap water	0	$1 \times 10^{-6}$	$0.96 \times 10^{-6}$	96.0	4.43
		$5 \times 10^{-6}$	$5.08 \times 10^{-6}$	101.6	1.66
		$1 \times 10^{-5}$	$0.98 \times 10^{-5}$	98.0	3.13
Spinach	0	$1 \times 10^{-6}$	$0.98 \times 10^{-6}$	98.0	2.88
		$5 \times 10^{-6}$	$4.93 \times 10^{-6}$	98.6	2.25
		$1 \times 10^{-5}$	$1.05 \times 10^{-5}$	105.0	1.92

#### 4. CONCLUSION

In this study, COF-DhaTab was prepared by Schiff base condensation reaction on the surface of MWCNTs as a carrier, and the COF@MWCNTs was employed to construct a novel electrochemical AChE biosensor for the sensitive detection of malathion. The COF@MWCNTs played a dual functional role of effective enzyme immobilization matrix and electrochemical signal enhancing material. The AChE/COF@MWCNTs/GCE biosensor showed a wide linear range ( $10^{-9}$  to  $10^{-5}$  M) and a low detection limit (0.5 nM) for quantitative analysis of malathion. The core-shell COF@MWCNTs composite provided a novel electrochemical biosensing platform for enzyme biosensors. The proposed biosensor in this work shows great promise for organophosphorus pesticide determination in environmental monitoring and food safety.

#### ACKNOWLEDGMENTS

This work was supported by the National Natural Science Foundation of China (21707014).

#### References

1. Y.P. Liu, S.Q. Liu, Y. Zhang, D.M. Qin, Z.T. Zheng, G.Y. Zhu, Y.T. Lv, Z.Q. Liu, Z. Dong, X.L.

- Liao, X.G. Li, *Food Control*, 107(2020) 106754.
2. H. Chen, J.Q. Zhu, Z. Li, A. Chen, Q. Zhang, *Environ. Monit. Assess.*, 188(2016) 614.
  3. V. Mahdavi, M.E.S. Heris, M. Dastranj, M.M. Farimani, Z. Eslami, H.Y. Aboul-Enein, *Water Air and Soil Pollution*, 232(2021) 159.
  4. S. Duttagupta, A. Mukherjee, A. Bhattacharya, J. Bhattacharya, *Sci. Total Environ.*, 717(2020) 137187.
  5. A.M. Badr, *Environ. Sci. Pollut. Res.*, 27(2020) 26036-26057.
  6. R. Anjitha, A. Antony, O. Shilpa, K.P. Anupama, S. Mallikarjunaiah, H.P. Gurushankara, *Environ. Res.*, 182(2020) 109131.
  7. W.R. Wang, X.X. Wang, N. Cheng, Y.B. Luo, Y.H. Lin, W.T. Xu, D. Du, *Trac-Trends Anal. Chem.*, 132(2020) 116041.
  8. N. Kalyani, S. Goel, S. Jaiswal, *Environ. Chem. Lett.*, 19(2021) 345-354.
  9. A.V. Alex, A. Mukherjee, *Microchem. J.*, 161(2021) 105779.
  10. C.S. Pundir, A. Malik, Preety, *Biosens. Bioelectron.*, 140(2019) 5-17.
  11. X.L. Zhang, G.L. Li, D. Wu, B. Zhang, N. Hu, H.L. Wang, J.H. Liu, Y.N. Wu, *Biosens. Bioelectron.*, 145(2019) 111699.
  12. F.L. Oliveira, A.D. Franca, A.M. de Castro, R. de Souza, P.M. Esteves, R.S.B. Goncalves, *ChemPlusChem*, 85(2020) 2051-2066.
  13. J.S. Gan, A.R. Bagheri, N. Aramesh, I. Gul, M. Franco, Y.Q. Almulaiky, M. Bilal, *Int. J. Biol. Macromol.*, 167(2021) 502-515.
  14. S. Kandambeth, V. Venkatesh, D.B. Shinde, S. Kumari, A. Halder, S. Verma, R. Banerjee, *Nat. Commun.*, 6(2015) 6786.
  15. X.J. Zhao, P. Pachfule, A. Thomas, *Chem. Soc. Rev.*, 50(2021) 6871-6913.
  16. Y.F. Sun, G.I.N. Waterhouse, L.H. Xu, X.G. Qiao, Z.X. Xu, *Sens. Actuator B-Chem.*, 321(2020) 128501.
  17. L.Y. Wang, Y. Xie, Y.X. Yang, H.H. Liang, L. Wang, Y.H. Song, *ACS Appl. Nano Mater.*, 3(2020) 1412-1419.
  18. L.L. Wang, C.X. Yang, X.P. Yan, *Sci. China-Chem.*, 61(2018) 1470-1474.
  19. A. Halder, S. Kandambeth, B.P. Biswal, G. Kaur, N.C. Roy, M. Addicoat, J.K. Salunke, S. Banerjee, K. Vanka, T. Heine, S. Verma, R. Banerjee, *Angew. Chem. Int. Ed.*, 55(2016) 7806-7810.
  20. F. Zhou, Y. Wang, W. Wu, T. Jing, S.R. Mei, Y.K. Zhou, *Sci. Rep.*, 6(2016) 38000.
  21. H.Y. Zuo, Y. Li, Y.Z. Liao, *ACS Appl. Mater. Interfaces*, 11(2019) 39201-39208.
  22. J. Chen. N. L, J.H. Liu, F.P. Zheng, *Microchem. J.*, 159(2020) 105460.
  23. X.-P. Lin, X.-Q. Wang, J. Wang, Y.-W. Yuan, S.-S. Di, Z.-W. Wang, H. Xu, H.-Y. Zhao, C.-S. Zhao, W. Ding, P.-P. Qi, *J. Chromatogr. A*, 1627(2020) 461387.
  24. X. Zhang, Z. Wang, L. Yao, Y.Y. Mai, J.Q. Liu, X.L. Hua, H. Wei, *Mater. Lett.*, 213(2018) 143-147.
  25. T. Itsoponpan, C. Thanachayanont, P. Hasin, *Sens. Actuator B-Chem.*, 337(2021) 129775.
  26. R.P. Luo, Z.J. Feng, G.N. Shen, Y. Xiu, Y.K. Zhou, X.D. Niu, H.S. Wang, *Sensors*, 18(2018) 12.
  27. E. Mahmoudi, H. Fakhri, A. Hajian, A. Afkhami, H. Bagheri, *Bioelectrochem.*, 130(2019) 107348.
  28. S. Wu, F.F. Huang, X.Q. Lan, X.Y. Wang, J.M. Wang, C.G. Meng, *Sens. Actuator B-Chem.*, 177(2013) 724-729.
  29. Y.P. Li, Y.F. Bai, G.Y. Han, M.Y. Li, *Sens. Actuator B-Chem.*, 185(2013) 706-712.
  30. Y. Chen, Y.Y. Zhu, Y.H. Zhao, J. Wang, *Food Chem.*, 345(2021) 128560.
  31. P. Liu, X. Li, X.C. Xu, X.H. Niu, M.Z. Wang, H.J. Zhu, J.M. Pan, *Sens. Actuator B-Chem.*, 338(2021) 129866.
  32. X. Dan, R.Y. Li, Q.S. Wang, Y.Q. Yang, H.Y. Zhu, Z.J. Li, *New J. Chem.*, 45(2021) 7129-7137.
  33. Q.S. Chen, R. Sheng, P.Y. Wang, Q. Ouyang, A.C. Wang, S. Ali, M. Zareef, M.M. Hassan, *Spectroc. Acta Pt. A-Molec. Biomolec. Spectr.*, 241(2020) 118654.
  34. M. Wang, K. Su, J. Cao, Y.X. She, A.M. Abd El-Aty, A. Hacimuftuoglu, J. Wang, M.M. Yan, S.H. Hong, S.B. Lao, Y.L. Wang, *Talanta*, 192(2019) 295-300.

35. M. Guler, V. Turkoglu, Z. Basi, *Electrochim. Acta*, 240(2017) 129-135.
36. S. Li, L. Qu, J.F. Wang, X.Q. Ran, X. Niu, *Int. J. Electrochem. Sci.*, 15(2020) 505-514.
37. C.S. Kushwaha, S.K. Shukla, *J. Mater. Sci.*, 54(2019) 10846-10855.
38. G. Bolat, S. Abaci, *Sensors*, 18(2018) 773.
39. N.F.M. Rodrigues, S.Y. Neto, R.D.S. Luz, F.S. Damos, H. Yamanaka, *Biosensors-Basel*, 8(2018) 16.
40. H. Ali, E. Khan, I. Ilahi, *J. Chem.*, 2019(2019) 6730305.
41. W.W. Dong, Y. Zhang, X. Quan, *Chemosphere*, 242(2020) 125113.
42. H.Y. Zhang, X.Z. Yuan, T. Xiong, H. Wang, L.B. Jiang, *Chem. Eng. J.*, 398(2020) 125657.
43. M. Ishaq, N. Sultana, M. Ikram, A. Iqbal, F. Shah, M. Hamayun, A. Hussain, *Arab. J. Geosci.*, 13(2020) 627.
44. M. Kovac, M. Bulaic, J. Jakovljevic, A. Nevistic, T. Rot, T. Kovac, I.D. Sarkanj, B. Sarkanj, *Microorganisms*, 9(2021) 216.

© 2022 The Authors. Published by ESG ([www.electrochemsci.org](http://www.electrochemsci.org)). This article is an open access article distributed under the terms and conditions of the Creative Commons Attribution license (<http://creativecommons.org/licenses/by/4.0/>).